INSTITUTE OF PHYSICS PUBLISHING JOURNAL OF PHYSICS A: MATHEMATICAL AND GENERAL

J. Phys. A: Math. Gen. **36** (2003) 1–15 PII: S0305-4470(03)61055-3

Polynomial combinatorial optimization methods for analysing the ground states of disordered systems

Heiko Rieger

Theoretische Physik, Universität des Saarlandes, 66041 Saarbrücken, Germany

Received 19 March 2003
Published DD MMM 2003
Online at stacks.iop.org/JPhysA/36/1

Abstract

We discuss the application of polynomial combinatorial optimization algorithms to extract the universal zero-temperature properties of various disordered systems. Dijkstras algorithm is used for models of non-directed elastic lines on general regular graphs with isotropically correlated random potentials. The successive shortest path algorithm for minimum-cost-flow problems is applied for the study of ground state properties and the entanglement of many elastic lines in a disordered environment and the disorder-induced loop percolation transition in a vortex glass model. The pre-flow-push algorithm for minimum-cut–maximum-flow problems is used for the investigation of a roughening transition occurring in a model for elastic manifolds in a periodic potential in the presence of point disorder.

PACS numbers: 74.60.Ge, 05.40.−a

(Some figures in this article are in colour only in the electronic version)

1. Introduction

Solid materials which contain a substantial degree of quenched disorder, so-called disordered systems, have been an experimental and a theoretical challenge for physicists for many decades. The different thermodynamic phases emerging in random magnets, the aging properties and memory effects of spin glasses, the disorder-induced conductor-to-insulator transition in electronic or bosonic systems, the collective behaviour of magnetic flux lines in amorphous high-temperature superconductors and the roughening transition of a disordered charge density wave systems, are only a few examples for these fascinating phenomena that occur due to the presence of quenched disorder.

Analytic studies of models for these systems are usually based on perturbation theories valid for weak disorder, on phenomenological scaling pictures or on mean-field approximations. Therefore the demand for efficient numerical techniques that allow the investigation of the model Hamiltonians of disordered systems has always been high. Three facts make life difficult here: (1) the regimes, where disorder effects are most clearly

0305-4470/03/000001+15$30.00

seen, are at low temperatures—and are even best visible at zero temperature; (2) the presence of disorder slows the dynamics of these systems down, they become *glassy*, such that for instance conventional Monte Carlo or molecular dynamics simulations encounter enormous equilibration problems; (3) any numerical computation of disordered systems has to incorporate an extensive disorder average.

In recent years more and more model systems with quenched disorder were found that can be investigated numerically (1) at zero temperature, (2) without equilibration problems, (3) extremely fast, in polynomial time (for a review on these developments see [1, 2] and [3] for an introduction to the non-expert). This *is* indeed progress, which became possible by the application of *exact* combinatorial optimization algorithms developed by mathematicians and computer scientists over the last few decades. This gift is not for free: first a mapping of the problem of finding the *exact* ground state of the model Hamiltonian under consideration onto a standard combinatorial optimization problem has to be found. If one is lucky, this problem falls into the class of *P*-problems, for which polynomial algorithms exist. If not, the intellectual challenge for the theoretical physicist remains to reformulate the model Hamiltonian in such a way that its universality class is not changed but a mapping on a *P*-problem becomes feasible.

In this paper, we review some of the most fruitful applications of polynomial algorithms from the realm of combinatorial optimization to various problems in the statistical physics of disordered systems. The next section presents the application of Dijkstras algorithm for finding shortest paths in weighted networks to the model of a non-directed polymer in a disordered environment with isotropical correlations. Then, in sections 3 and 4, we discuss minimum-cost-flow problem on weighted graphs and its solution via the successive shortest path algorithm and apply it to the entanglement transition of elastic lines in a disordered environment and to the loop percolation transition in a vortex glass model. In section 5 we focus on the minimum-cut–maximum-flow problem and discuss among its many applications the roughening transition of elastic media in a disordered environment. A discussion closes this paper in section 6.

2. Polymers in a disordered environment and Dijkstras algorithm

A well-studied model of a single elastic line [4], like an individual polymer or a single magnetic flux line in a type II superconductor, in a disordered environment is the following: if one excludes overhangs (and by this also self-overlaps) of the elastic line one can parametrize its configuration by the longitudinal coordinate z. The line configuration can then be described by the transverse coordinate $\mathbf{r}(z)$ as a function of z. The presence of disorder is usually modelled by a random potential energy $V(\mathbf{r}, z)$ and the ground state configuration of the line is highly non-trivial due to the competition between the elastic energy, that tends to straighten the line, and the random energy, that tries to bend the line into positions of favourable energy,

$$\mathcal{H}_{\text{single-line}} = \mathcal{H}_{\text{elastic}} + \mathcal{H}_{\text{random}} = \int_0^H \mathrm{d}z \left\{ \frac{\gamma}{2} \left[\frac{\mathrm{d}\mathbf{r}}{\mathrm{d}z} \right]^2 + V[\mathbf{r}(z), z] \right\} \tag{1}$$

where H is the longitudinal length (not the proper length) of the line. The random potential energy is a Gaussian variable with prescribed mean and correlations $\langle\langle V[\mathbf{r}, z]V[\mathbf{r}', z']\rangle\rangle = g(\mathbf{R} - \mathbf{R}')$, where $\mathbf{R} = (\mathbf{r}, z)$ and $\langle\langle \cdots \rangle\rangle$ denotes the average over the disorder.

A lattice version of this continuum model is the *directed* polymer model: the lines correspond to directed paths on a hyper-cubic lattice that start at a specific lattice site, say $(0, 0, \ldots, 0)$ and proceed only in the $(1, 1, \ldots, 1)$ direction along the bonds. The energy contribution for a path passing bond $\mathbf{i}$ of the lattice is a *positive* random variable $e_{\mathbf{i}}$ and the

total energy of a path $\mathcal{P}$ is simply

$$\mathcal{H}^{\text{lattice}}_{\text{single-line}} = \sum_{\mathbf{i}\in\mathcal{P}} e_{\mathbf{i}} = \sum_{\mathbf{i}} e_{\mathbf{i}} n_{\mathbf{i}} \tag{2}$$

where $n_{\mathbf{i}} = 1$ if the path passes bond $\mathbf{i}$ (i.e. $\mathbf{i} \in \mathcal{P}$) and $n_{\mathbf{i}} = 0$ otherwise.

We are interested in isotropically correlated disorder and consider the problem on a *non-directed* (square) lattice (i.e. paths can pass any bond in both directions) in order not to exclude overhangs right from the beginning. In case of uncorrelated disorder overhangs were shown to be irrelevant [6], but for isotropically correlated disorder this is not clear. We define the latter to decay algebraically with the spatial distance of the bonds

$$\langle\langle e_{\mathbf{i}} - e_{\mathbf{j}} \rangle\rangle = |\mathbf{R}_{\mathbf{i}} - \mathbf{R}_{\mathbf{j}}|^{2\alpha-1} \tag{3}$$

where $\mathbf{R}_{\mathbf{i}}$ is the spatial position of bond $\mathbf{i}$, and we generate correlated random numbers using a well-established numerical procedure [5].

We calculate the exact ground states of the Hamiltonian (2) or optimal paths using Dijkstras algorithm (note that all energies $e_{\mathbf{i}}$ are positive). This simple polynomial algorithm works as follows: let $V = \{1, \ldots, L^d\}$ be the set of lattice sites and $A = \{(i, j)|i, j \in V \text{ nearest neighbours}\}$ the set of bonds. The algorithm increases successively a subset S of sites for which the optimal path starting at the fixed site s is known. Obviously initially $S := \{s\}$. We denote the energy of the optimal path starting at s and terminating at i with $E(i)$ and since all optimal paths can be constructed via a predecessor list, we keep track of this list, too, via an array $pred(i)$, denoting the predecessor site of site i in a shortest path from s to i:

algorithm Dijkstras
begin
  $S := \{s\}$; $\bar{S} := V \backslash \{s\}$;
  $E(s) := 0$, $pred(s) := 0$;
  while $|S| < |V|$ **do**
  begin
    choose $(i, j) : E(j) := \min_{k,m}\{E(k) + e_{(k,m)} \mid k \in S, m \in \bar{S}, (k, m) \in A\}$;
    $\bar{S} := \bar{S} \backslash \{j\}$; $S := S \cup \{j\}$;
    $pred(j) := i$;
  end
end

In figure 1 we show examples of the set $\{i\}$ of lattice sites that are end points of optimal paths starting from a fixed initial site and having a total energy $E(i)$ less than a given value $E_{\max}$. For uncorrelated disorder the surface of this set is roughly a semi-circle, whereas for strongly correlated disorder the surface becomes topologically more complicated.

The universal properties of the optimal paths are typically described by the scaling of two characteristic quantities: the average transverse fluctuations $\langle\langle \mathbf{r}^2 \rangle\rangle \propto H^{\nu}$ and the energy fluctuations $\langle\langle E^2 \rangle\rangle \propto H^{\omega}$, where H is the longitudinal distance between starting point and end point of the paths. By computing the optimal paths for several thousands of samples for a given disorder correlation exponent α and for a given longitudinal distances H and fitting the resulting data for transverse and energy fluctuations to the expected power laws, we can extract the exponents ν and ω (the details of these computations will be published elsewhere [7]). The resulting estimates in 2D are shown in figure 2 [7]. Although the number of overhangs in the optimal paths we computed in the non-directed case increased with α (i.e. increasing correlations) the fraction of bonds contributing to overhangs scaled to zero for all values of α we considered. Hence overhangs appear to be irrelevant also in the presence of correlated disorder.

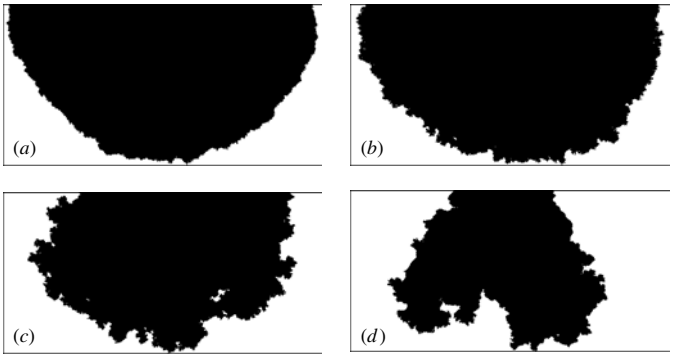

Figure 1. Example for the growth front of the non-directed polymer for uncorrelated disorder ((*a*) and (*b*)) and correlated disorder ((*c*) and (*d*); $\alpha = 0.4$). The black pixels indicate the lattice sites of the (square) lattice that are connected via optimal paths to the offspring (centre of the top line) with energy less than a given value.

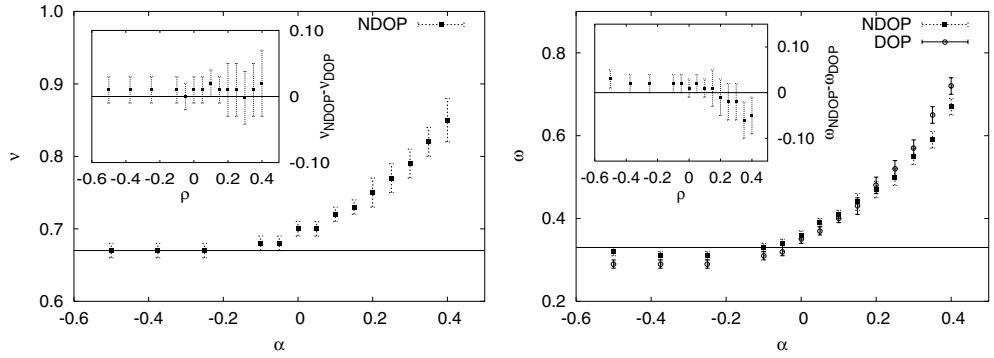

Figure 2. Numerical estimate of the roughness exponent ν (left) and energy fluctuation exponent ω (right) as a function of the correlation exponent α. The straight lines are at exactly known values $\nu = 2/3$ and $\omega = 1/3$ for uncorrelated disorder. Around $\alpha = 0$ the correlations of the disorder become relevant. The insets show the difference of our estimates between the directed and non-directed case.

3. Entanglement transition of elastic lines in a disordered environment

When one puts interacting elastic lines together into a finite system with a given density of lines they will show interesting collective behaviour. Examples are the entanglement of magnetic flux lines in high-T_c superconductors in the mixed phase [8] and the entanglement of polymers in materials such as rubber [9]. The degree of entanglement of the lines usually manifests itself in various measurable properties such as stiffness or shear modulus in the case of polymers and in transport or dynamical properties for magnetic flux lines in superconductors. A theoretical description of these line systems can be based on the single-line Hamiltonian (1) plus an appropriate line interaction term,

$$\mathcal{H}_{\text{many-lines}} = \sum_{i=1}^{N} \mathcal{H}^{(i)}_{\text{single-line}} + \sum_{i<j} \int_0^L \mathrm{d}z \int_0^L \mathrm{d}z'\, V_{\text{int}}[\mathbf{R}_i(z) - \mathbf{R}_j(z')] \qquad (4)$$

where $\mathbf{R}_i(z) = (\mathbf{r}_i(z), z)$ is the spatial position of the infinitesimal line segment $\mathrm{d}z$ of the ith line. If the interactions $V_{\text{int}}[\mathbf{R}_i(z) - \mathbf{R}_j(z')]$ are short ranged (i.e. in case of flux lines the

screening length is small compared to the average line distance) or just hard-core repulsive, and the random, δ-correlated disorder potential $V_r[\mathbf{r}_i(z), z]$ in (1) is strong compared to the elastic energy ($\propto \gamma$) this continuum model reduces to a lattice model reminiscent of the single-line lattice model (2),

$$\mathcal{H}^{\text{lattice}}_{\text{many-lines}} = \sum_{\mathbf{i}} e_{\mathbf{i}} n_{\mathbf{i}} \tag{5}$$

where $n_{\mathbf{i}} = 1$ if a line passes bond $\mathbf{i}$ and $n_{\mathbf{i}} = 0$ otherwise and the *positive* random variable $e_{\mathbf{i}}$ is the energy cost for a line segment to occupy bond $\mathbf{i}$. The hard-core constraint is thus enforced on the bonds but for the sake of an easier formal description we allow the lines to touch in isolated points, the lattice sites. The lines live on the bonds of a simple cubic lattice with a lateral width L and a longitudinal height H ($L \times L \times H$ sites) with free boundary conditions in all directions. Each line starts and ends at an arbitrary position on the bottom respective top planes. The number N of lines threading the sample is fixed by a prescribed density $\rho = N/L^2$. For a single line $N = 1$, one recovers the non-directed polymer model (2). The random bond energies are uniformly distributed over the interval [0, 1].

Note that the allowed configurations of the bond variables $n_{\mathbf{i}}$ are only those that are identified with lines threading the samples (or loops inside the sample, which, however, cost energy and therefore do not occur in the ground state), which means that the number of occupied bonds connected to a lattice site that lies neither on the top nor on the bottom plane has always to be even. If we connect all sites on the top to an extra site, called the source, and all sites on the bottom to another extra site, called the target, then the latter statement remains true also for the top and bottom plane. We can now say that N lines start at the source node and terminate at the target node, or, in network flow jargon, the feasible configurations of the variables $n_{\mathbf{i}}$ constitute a flow with zero excess on all lattice sites and an excess $+N$ and $-N$ for the source and target nodes, respectively.

Thus the determination of the ground state configuration of the N-line problem with the Hamiltonian (5) is a minimum-cost-flow problem, which can be solved with a successive shortest path algorithm [1–3]. In essence one starts with the zero flow $n_{\mathbf{i}} = 0$, corresponding to zero lines in the system, and sends successively one unit of flow from the source to the target, corresponding to adding one line after the other to the system. This has to happen with the minimal energy, i.e. along optimal paths, which are calculated using Dijkstras algorithm that we encountered already in the single-line problem discussed in the last section. However, when trying to add a line to a system with a number, say M, of lines already present, the existing line configuration sometimes must be changed to minimize the total energy for $M + 1$ line solution. That becomes feasible by allowing flow to be sent *backwards* on already occupied bonds. By this operation one *gains* energy (whereas occupying an empty bond $\mathbf{i}$ always costs energy $e_{\mathbf{i}} \geqslant 0$), which means one has to operate on a network that has to be adapted to the existing flow configuration and has negative energies on all occupied bonds. Unfortunately, Dijkstras algorithm works only for positive bond energies, and one has to use either a slower (label-correcting) algorithm to find the optimal paths in a graph with negative edge costs [3] or the concept of node potentials, by which one can make all energies in the adapted network non-negative without changing the actual shortest paths. This procedure is described in full detail in [3].

The resulting line configuration is then analysed. We compute the winding angle of all line pairs as indicated in figure 3 (cf [10]). For each z-coordinate the vector connecting the two lines is projected onto that basal plane (left part of figure 3). $z = 0$ gives the reference line with respect to which the consecutive vectors for increasing z-coordinate have an angle $\phi(z)$. If the two lines intersect we neglect the intersection point and interpolate between the last and the next point in such a way that the global winding angle is minimized. We define two lines

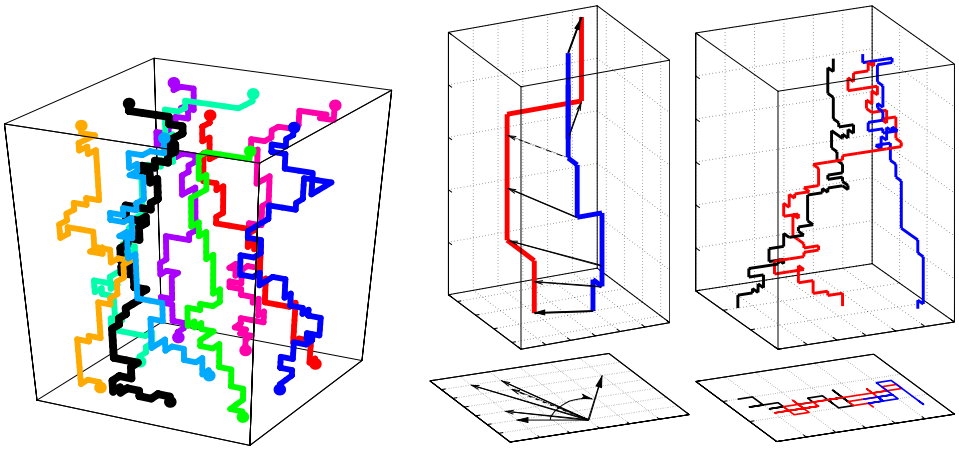

Figure 3. Left: ground state configuration of a N-line system with $N = 9$ defined by (5). The entry/exit points are fixed in a regular 3×3 array for better visibility. Right: definition of the winding angle of two flux lines. Right part, top: a configuration of three lines that are entangled. Right part, bottom: the projection of the line configuration on the basal plane, defining a connected cluster.

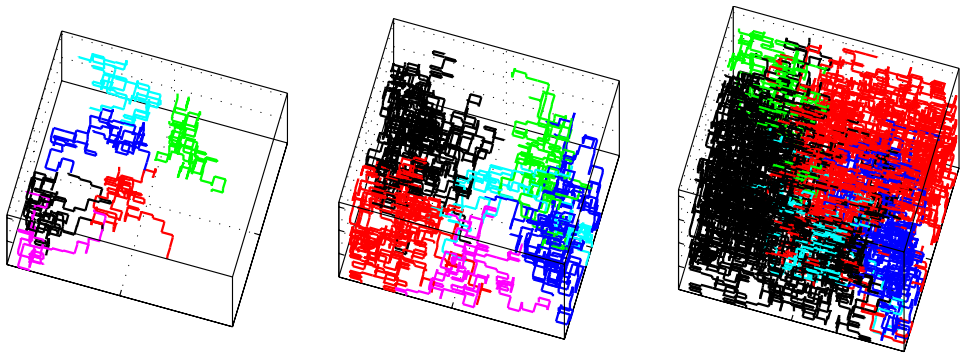

Figure 4. Line configurations for different heights H (from left to right: $H = 64, 96, 128$), the lateral size $L = 20$, the line density is $\rho = 0.3$. Only the largest line bundles are shown, indicated by a varying grey scale. Black denotes the largest cluster, which eventually percolates.

to be *entangled* when $\phi(z) > 2\pi$. This choice is one that measures entanglement from the topological perspective [11], and comes from the requirement that an entangled pair of lines cannot be separated by a suitable linear transformation in the basal plane (i.e. the lines almost always would cut each other, if one were shifted). The precise definition of entanglement is not of major relevance, and the one used is useful since it is the computationally easiest.

Sets or *bundles* of pairwise entangled lines are formed so that a line belongs to a bundle if it is entangled at least with one other line in the set. The topological multi-line entanglement could be characterized by other measures as well; the universal properties of the transition will not depend on these. These line bundles are spaghetti-like, i.e., topologically complicated and knotted sets of one-dimensional objects. To study the size distribution of these objects we project these bundles on the basal plane, as indicated in figure 3, where a bundle projects onto a connected cluster. The probability for two lines to be entangled increases with increasing system height. Consequently, one would expect that the bundle size increases with H, and therefore also their projections, the clusters. This scenario is exemplified in figure 4, for

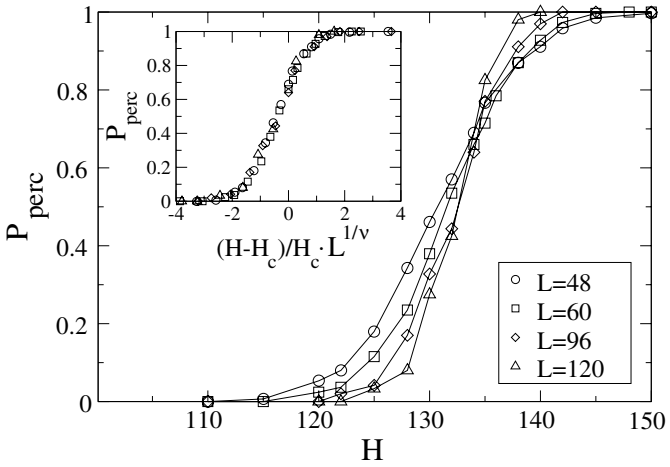

Figure 5. Percolation probability for different lateral system sizes L as a function of the system height H, the line density is $\rho = 0.3$. Inset: scaling plot of the data with $H_c = 134$ and $\nu = 4/3$.

the largest height the largest cluster spans from one side of the system to the other, i.e. it *percolates*.

Hence, for a given line density ρ we expect that for system heights larger than a critical value H_c a system spanning large entangled bundle occurs, containing an infinite number of lines in the limit $L \to \infty$. We will call this an *entanglement transition* occurring at a finite system height H_c. In the projection plane this appears like a percolation transition and in the following we will investigate its universal properties.

The numerical data we present have been obtained by averaging over up to 10^3 realizations of the random potentials e_i in (5) and the statistical error resulting from this finite sample average is in all cases smaller than the symbol size. We studied different line densities between $\rho = 0.1$ and $\rho = 0.5$, but present for brevity only data for $\rho = 0.3$. In figure 5 we show the probability P_{perc} of the clusters, formed by the entangled bundles in the projection plane, to percolate as a function of the height H of the system. The curves for different lateral system sizes L intersect at H_c, which gives our estimate for $H_c(\rho = 0.3) = 134$. The inset shows a scaling plot according to

$$P_{\text{perc}} = p(L^{1/\nu}\delta) \tag{6}$$

with $\delta = (H - H_c)/H_c$ the reduced distance from the critical height and $\nu = 4/3$ the correlation length exponent. The finite size corrections for smaller system sizes than those shown are large, but could be incorporated in the scaling plot by using an L-dependent shift $H_c(L)$ that converges to H_c for larger L.

$\nu = 4/3$ is the exponent of conventional bond percolation in two dimensions. Thus we are led to the conclusion that the entanglement transition belongs to the same universality class as conventional two-dimensional (2D) percolation. We checked other quantities to confirm this result. The cluster size distribution $P(n)$ at $H = H_c$ approaches $P(n) \propto n^{-\tau}$ with $\tau = 187/91 \approx 2.055$ in the limit $L \to \infty$. The mass (i.e. number of entangled lines) of the percolating bundle at H_c fits well to $M \propto L^{d_f}$ with $d_f = 91/48 \approx 1.896$. Both exponents, the cluster distribution exponent τ and the fractal dimension d_f, are identical to those for conventional bond percolation and one can also use the order parameter exponent, $\beta = 5/36$, to fit the data reasonably well. Details of these computations will be published elsewhere [12].

4. Disorder-induced loop percolation in vortex glasses

Another application of the successive shortest path algorithm for minimum-cost-flow problems is finding the ground state of the Hamiltonian

$$H = \sum_{\mathbf{i}} (n_{\mathbf{i}} - b_{\mathbf{i}})^2 \quad \text{with the constraint} \quad \forall k : \sum_{l \text{ n.n. of } k} n_{(kl)} = 0 \tag{7}$$

where the integer variables $n_{\mathbf{i}}$ live on the bonds $\mathbf{i}$ of a d-dimensional hyper-cubic lattice and $b_{\mathbf{i}} \in [-2\sigma, 2\sigma]$ are real valued quenched random variables with $\sigma \geqslant 0$ setting the strength of the disorder. The constraint $\sum_{l \text{ n.n. of } k} n_{(kl)} = 0$ means that at all lattice sites k the incoming flow has to balance the outgoing flow, i.e. the flow $\{n_{\mathbf{i}}\}$ is divergenceless. The physical motivation of studying these kinds of models is the following.

In 2D the Hamiltonian (7) occurs for instance in the context of the solid-on-solid (SOS) model on a disordered substrate [13]. The SOS representation of a 2D surface is defined by integer height variables u_k for each lattice site k of a square lattice. The disordered substrate is modelled via random offsets $d_k \in [0, 1]$ for each lattice site, such that the total height at lattice site k is $h_k = u_k + d_k$. The total energy of the surface is

$$\mathcal{H}_{\text{SOS}} = \sum_{(kl)} (h_k - h_l)^2 = \sum_{(\tilde{kl})} (n_{(\tilde{kl})} - b_{(\tilde{kl})})^2 \tag{8}$$

where the first sum runs over all nearest neighbour pairs (kl) of the square lattice and the second sum runs over all bonds $(\tilde{kl})$ of the *dual* lattice (being a square lattice, too), which connect the centres of the elementary plaquettes of the original lattice. A dual bond $(\tilde{kl})$ therefore crosses perpendicularly a bond (kl) connecting neighbours k and l on the original lattice. We define $n_{(\tilde{kl})} = n_k - n_l$ and $d_{(\tilde{kl})} = d_l - d_k$ if l is either the right or the upper neighbour of k (i.e. for $k = (x, y)$ either $l = (x + 1, y)$ or $l = (x, y + 1)$) and $n_{(\tilde{kl})} = n_l - n_k$ and $d_{(\tilde{kl})} = d_k - d_l$ if l is either the left or the lower neighbour of k (i.e. for $k = (x, y)$ either $l = (x - 1, y)$ or $l = (x, y - 1)$). In this way, the sum over all four dual bond variables attached to one site of the dual lattice corresponds to the sum of original height variables around elementary plaquettes in the original lattice, $(n_{(x,y)} - n_{(x,y+1)}) + (n_{(x,y+1)} - n_{(x+1,y+1)}) + (n_{(x+1,y+1)} - n_{(x+1,y)}) + (n_{(x+1,y)} - n_{(x,y)}) = 0$, which implies that the flow $\{n_{(\tilde{kl})}\}$ is divergence free as inferred in (7).

In 3D the Hamiltonian (7) is the strong screening limit of the vortex glass model for disordered superconductors [14, 15]

$$\mathcal{H}_{\text{VG}} = \sum_{i,j} (n_i - b_i) G_\lambda(\mathbf{r}_i - \mathbf{r}_j)(n_j - b_j) \tag{9}$$

where the integer vortex variables n_i live on the bonds of a simple cubic lattice and have to fulfil the constraint in (7) since they represent magnetic vortex lines that are divergence free. The real-valued quenched random variables $b_i \in [-2\sigma, 2\sigma]$ are derived from the lattice curl of a random vector potential ($\sigma \geqslant 0$ being the strength of the disorder). The three-dimensional (3D) vector $\mathbf{r}_i$ denotes the spatial positions of bond i in the lattice and the sum runs over all bond pairs of the lattice (not only nearest neighbours). The lattice propagator $G_\lambda(\mathbf{r})$ has the asymptotic form $G_\lambda(\mathbf{r}) \propto \exp(-|\mathbf{r}|/\lambda)/|\mathbf{r}|$, where λ is the screening length. In the strong screening limit $\lambda \to 0$ only the on-site repulsion survives [14] and gets

$$\mathcal{H}_{\text{VG}}^{\lambda \to 0} = \sum_i (n_i - b_i)^2 \tag{10}$$

which is the Hamiltonian (7) in 3D that we intend to discuss here.

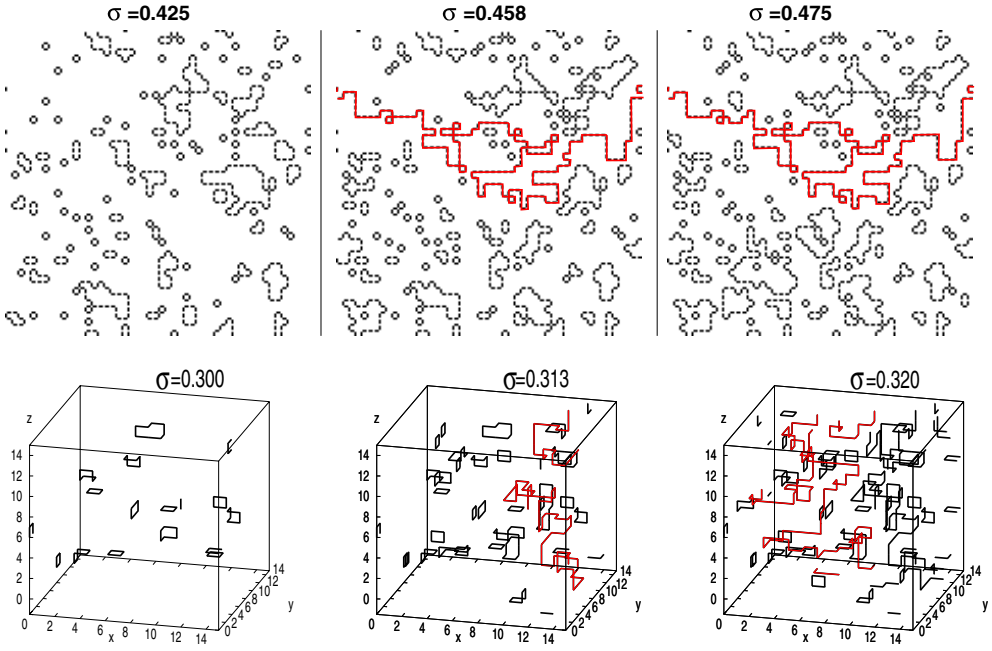

Figure 6. Examples of ground state configurations of the Hamiltonian (7) for varying disorder strengths σ (for particular disorder realizations). Top: 2D, $L = 50$, the critical disorder strength is $\sigma_c \approx 0.46$; bottom: 3D, $L = 16$, the critical disorder strength is $\sigma_c \approx 0.31$. The occupied bonds ($n_i \neq 0$) are marked black, the percolating loop is marked by light grey (red).

The ground state of (7) can again be computed within polynomial time by a successive shortest path algorithm [3]. As for the N-line problem one starts with a configuration $\{n_\mathbf{i}\}$ that optimizes the Hamiltonian in (7) but does not, in general, fulfil the mass balance constraint given in (7). In the N-line problem that was simply the zero-flow $n_\mathbf{i} = 0$, which does not fulfil the requirement that the source and the target have excess $+N$ and $-N$, respectively. Here we start with $n_\mathbf{i}$ the closest integer to the real number $b_\mathbf{i}$ for each bond $\mathbf{i}$. Since this solution violates the mass-balance constraint one successively sends flow from nodes that have an excess flow to nodes that have a deficit along optimal paths that are again found using node potentials (to make all costs non-negative) and Dijkstras algorithm. The details of this algorithm can be found in [1–3].

Figure 6 shows three typical ground state configurations for different strength of the disorder σ in 2D and in 3D. For small σ only small isolated loops occur, whereas for larger σ one finds loops that extend through the whole system, they percolate. A finite size scaling study of the underlying percolation transition yields a novel universality class with numerically estimated critical exponents (see figure 7) $\nu = 3.3 \pm 0.3$, $\beta = 1.8 \pm 0.4$ and $\tau = 2.45 \pm 0.05$ in 2D, and $\nu = 1.05 \pm 0.05$, $\beta = 1.4 \pm 0.1$ and $\tau = 2.85 \pm 0.05$ in 3D. Details of these calculations will be published elsewhere [16].

5. Elastic manifolds in a disordered environment and a periodic potential

A system of strongly interacting (classical) particles or other objects, like magnetic flux lines in a type II superconductor (as we discussed in section 3 and for which the starting Hamiltonian would be given by (4)) or a charge density wave system in a solid, will order

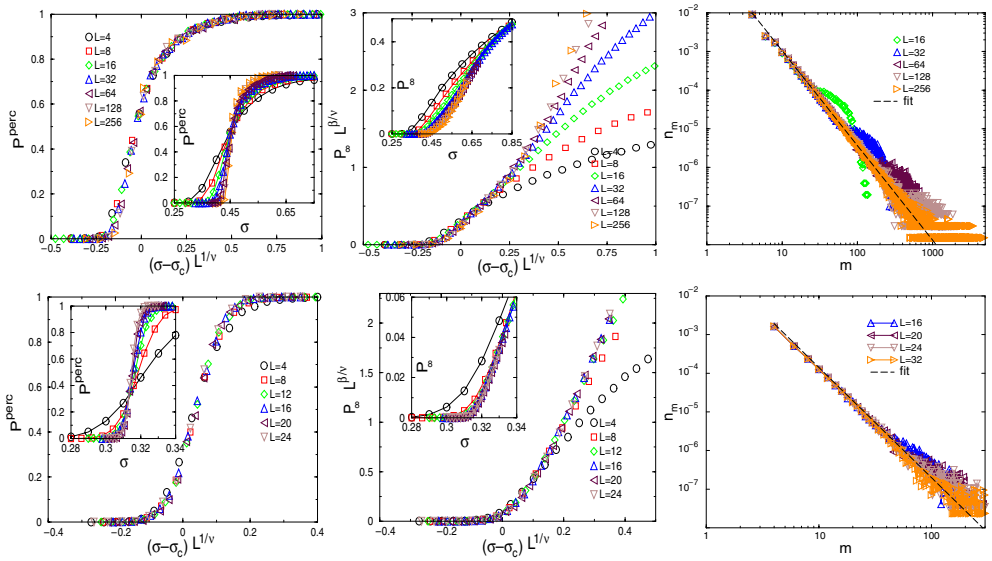

Figure 7. Finite size scaling analysis for the model (7) in 2D (top) and in 3D (bottom). Plot of the percolation probability $P^{\rm perc}$ (left) and of the probability P_∞ for a bond belonging to a percolating loop (middle). For 2D the best data collapse is obtained for $\nu = 3.3$, $\beta = 1.8$, for 3D it is $\nu = 1.05$, $\beta = 1.4$. The insets show the raw data. Right: plot of the average number n_m of loops of mass m per lattice bond at $\sigma_{\rm c} = 0.458$ in 2D and at $\sigma_{\rm c} = 0.3129$ in 3D, respectively. The straight line represents $n_m \propto m^\tau$, with $\tau = 2.45$ in 2D and $\tau = 2.85$ in 3D.

at low temperatures into a regular arrangement a lattice (crystal lattice or flux line lattice). Fluctuations either induced by thermal noise (temperature) or by disorder (impurities, pinning centres) induce deviations of the individual particles from their equilibrium positions. As long as these fluctuations are not too strong an expansion of the potential energy around these equilibrium configuration might be appropriate. An expansion up to second order is called the elastic description or elastic approximation, which in a coarse-grained form (where the individual particles that undergo displacements from their equilibrium positions do not occur any more and are replaced by a continuum field $\phi(\mathbf{r})$) then reads

$$\mathcal{H}_{\rm manifold} = \mathcal{H}_{\rm elastic} + \mathcal{H}_{\rm random} = \int {\rm d}^d\mathbf{r}\,\frac{\gamma}{2}|\nabla\phi(\mathbf{r})|^2 + V(\phi(\mathbf{r}),\mathbf{r}). \tag{11}$$

The random potential energy is a δ-correlated Gaussian variable with mean zero, $\langle\langle V(\phi,\mathbf{r})V(\phi',\mathbf{r}')\rangle\rangle = D^2\delta(\phi-\phi')\delta\mathbf{r}-\mathbf{r}')$. The integration extends over the whole space that paramtrizes the manifold, for instance $d = 1$ for an elastic line in a random potential, $d = 2$ for an interface or a surface in a disordered environment etc. Note that for $d = 1$ one recovers the single-line Hamiltonian (1). The many-line Hamiltonian (4) also allows such an elastic description in the limit, in which the interactions are strong and the random potential is weak compared to the elastic energy. In this limit the lines will only deviate moderately from a regular, translationally invariant configuration (the Abrikosov flux line lattice). This case is called an elastic periodic medium and one has to modify the ϕ-part of the disorder correlator such that the Hamiltonian has the correct translational symmetry [17].

The presence of a periodic background potential, like a crystal potential, has a smoothening effect on the elastic manifold and tends to lock it into one of its minima. The competition between the random potential, that roughens the manifold, and such a periodic potential might

lead to a roughening transition [18, 19]. In 2D this is actually not the case [20], but in 3D there is as we will see. We consider a lattice version of the Hamiltonian

$$\mathcal{H} = \mathcal{H}_{\text{manifold}} + H_{\text{periodic}} \quad \text{with} \quad H_{\text{periodic}} = \int \mathrm{d}^d \mathbf{r}\, V_{\text{periodic}}(\phi(\mathbf{r})) \tag{12}$$

where $V_{\text{periodic}}(\phi) = -\cos\phi$ represents the periodic potential.

We introduce a discrete solid-on-solid (SOS) type interface model for the elastic manifold whose continuum Hamiltonian is given in equation (12). Locally, the EM remains flat in one of periodic potential minima at $\phi = 2\pi h$ with integer h. Due to fluctuations, some regions might shift to a different minimum with another value of h to create a step (or domain wall) separating domains. To minimize the cost of the elastic and periodic potential energy in equation (12), the domain-wall width must be finite, say ξ_o. Therefore, if one neglects fluctuations in length scales less than ξ_o, the continuous displacement field $\phi(\mathbf{r})$ can be replaced by the integer height variable $\{h_{\mathbf{x}}\}$ representing a (3 + 1)-dimensional SOS interface on a simple cubic lattice with sites $\mathbf{x} \in \{1, \ldots, L\}^3$. The lattice constant is of order ξ_o and set to unity. The energy of the interface is given by the Hamiltonian

$$\mathcal{H} = \sum_{\langle \mathbf{x},\mathbf{y}\rangle} J_{(h_{\mathbf{x}},\mathbf{x});(h_{\mathbf{y}},\mathbf{y})} |h_{\mathbf{x}} - h_{\mathbf{y}}| - \sum_{\mathbf{x}} V_R(h_{\mathbf{x}}, \mathbf{x}) \tag{13}$$

where the first sum is over nearest neighbour site pairs. After the coarse graining, the step energy $J > 0$ as well as the random pinning potential energy V_R becomes a quenched random variable distributed independently and randomly. Note that a periodic elastic medium has the same Hamiltonian as in equation (13) with random but periodic J and V_R in h with periodicity p [21]. In this sense, the elastic manifold emerges as in the limit $p \to \infty$ of the periodic elastic medium.

To find the ground state, one maps the 3D SOS model onto a ferromagnetic random bond Ising model in (3 + 1)-dimensional hyper-cubic lattice with anti-periodic boundary conditions in the extra dimension [22] (for the 3-space direction one uses periodic boundary conditions instead). The anti-periodic boundary conditions force a domain wall into the ground state configuration of the (3 + 1)-dimensional ferromagnet. Note that bubbles are *not* present in the ground state. A domain wall may contain an overhang which is unphysical in the interface interpretation. Fortunately, one can forbid overhangs in the Ising model representation using a technique described in [22]. If the longitudinal and transversal bond strengths are assigned with $J/2$ and $V_R/2$ occurring in equation (13), respectively, this domain wall of the ferromagnet becomes equivalent to the ground state configuration of (13) for the interface with the same energy. The domain wall with the lowest energy is then determined exactly by using a combinatorial optimization algorithm, a so-called max-flow–min-cost algorithm [1–3].

For completeness we briefly sketch how to solve the task of finding the minimal energy configuration for an interface in a $(d + 1)$-dimensional random bond ferromagnet $H = \sum_{\langle ij\rangle} J_{ij}\sigma_i\sigma_j$ in which we fix all spins in the lower (upper) plane, i.e. all σ_i with $i = (x_1 1, \ldots, x_d, y)$ and $y = 1$ ($y = H$), to be $\sigma_i = +1$ (-1). First one maps it onto a flow problem in a capacitated network. We introduce two extra sites, a source node s, which we connect to all spins of the hyperplane $y = 1$ with bonds $J_{s,(x_1,\ldots,x_d,y=1)} = J_\infty$, and a sink node t, which we connect to all spins of the hyperplane $y = H$ with bonds $J_{s,(x_1,\ldots,x_d,y=H)} = J_\infty$. We choose $J_\infty = 2\sum_{(ij)} J_{ij}$, i.e. strong enough that the interface cannot pass through a bond involving one of the two extra sites. Now we enforce the aforementioned boundary conditions for the spins in the upper and the lower plane by simply fixing $\sigma_s = +1$ and $\sigma_t = -1$. The graph underlying the capacitated network we have to consider is now defined by the set of

vertices (or nodes) $N = \{1, \ldots, H \cdot L^d\} \cup \{s, t\}$ and the set of edges (or arcs) connecting them $A = \{(i, j) \,|\, i, j \in N, J_{ij} > 0\}$.

The capacities u_{ij} of the arcs (i, j) are given by the bond strength J_{ij}. For any spin configuration $\sigma = (\sigma_1, \ldots, \sigma_N)$ we define now $S = \{i \in N \,|\, \sigma_i = +1\}$ and $\bar{S} = \{i \in N \,|\, \sigma_i = -1\} = N \backslash S$. Obviously $\sigma_s \in S$ and $\sigma_t \in \bar{S}$. The knowledge of S is sufficient to determine the energy of any spin configuration via $H(S) = -C + 2\sum_{(i,j)\in(S,\bar{S})} J_{ij}$ where $(S, \bar{S}) = \{(i, j) \,|\, i \in S, j \in \bar{S}\}$. The constant $C = \sum_{(i,j)\in A} J_{ij}$ is irrelevant, i.e. independent of S. Note that $(S, \bar{S})$ is the set of edges (or arcs) connecting S with $\bar{S}$, which means it cuts N in two disjoint sets. Since $s \in S$ and $t \in \bar{S}$, this is a so-called *s–t*-cut-set, abbreviated as $[S, \bar{S}]$. Thus the problem of finding the ground state configuration of an interface in the random bond ferromagnet can be reformulated as a *minimum-cut* problem

$$\min_{S\subset N}\{H'(S)\} = \min_{[S,\bar{S}]} \sum_{(i,j)\in(S,\bar{S})} J_{ij} \tag{14}$$

in the above-defined capacitated network (with $H' = (H + C)/2$). It does not come as a surprise that this minimum cut is *identical* with the interface between the $(\sigma_i = +1)$-domain and the $(\sigma_i = -1)$-domain that has the lowest energy. Actually, any *s–t*-cut-set defines such an interface, some of them might consist of many components, which is of course energetically unfavourable.

A flow in the network G is a set of non-negative numbers x_{ij} subject to a capacity constraint and a mass-balance constraint for each arc

$$0 \leqslant x_{ij} \leqslant u_{ij} \quad \text{and} \quad \sum_{\{j|(i,j)\in A\}} x_{ij} - \sum_{\{j|(j,i)\in A\}} x_{ji} = \begin{cases} -v & \text{for} \quad i = s \\ +v & \text{for} \quad i = t \\ 0 & \text{else.} \end{cases} \tag{15}$$

This means that at each node everything that goes in has to go out, too, with the only exception being the source and the sink. What actually flows from s to t is v, the value of the flow. The *maximum-flow problem* for the capacitated network G is simply to find the flow $\mathbf{x}$ that has the maximum value v under the constraint (15).

Let $\mathbf{x}$ be a flow, v its value and $[S, \bar{S}]$ an *s–t*-cut. Then, by adding the mass balances for all nodes in S we have $v = \sum_{(i,j)\in(S,\bar{S})} x_{ij} - \sum_{(i,j)\in(\bar{S},S)} x_{ji}$ and since $x_{ij} \leqslant u_{ij}$ and $x_{ji} \geqslant 0$ the following inequality holds: $v \leqslant \sum_{(i,j)\in(S,\bar{S})} u_{ij} = u[S, \bar{S}]$. Thus the value of any flow $\mathbf{x}$ is less than or equal to the capacity of any cut in the network. If we discover a flow $\mathbf{x}$ whose value is equal to the capacity of some cut $[S, \bar{S}]$, then $\mathbf{x}$ is a maximum flow and the cut is a minimum cut. The following implementation of the augmenting path algorithm constructs a flow whose value is equal to the capacity of an *s–t*-cut it defines simultaneously. Thus it will solve the maximum-flow problem (and, of course, the minimum-cut problem).

Given a flow $\mathbf{x}$, the residual capacity r_{ij} of any arc $(i, j) \in A$ is the maximum additional flow that can be sent from node i to node j using the arcs (i, j) and (j, i). The residual capacity has two components: (1) $u_{ij} - x_{ij}$, the unused capacity of arc (i, j), (2) x_{ji} the current flow on arc (j, i), which we can cancel to increase the flow from node i to j, $r_{ij} = u_{ij} - x_{ij} + x_{ji}$. The residual network $G(\mathbf{x})$ with respect to the flow $\mathbf{x}$ consists of the arcs with *positive* residual capacities. An augmenting path is a directed path from the node s to the node t in the residual network. The *capacity of an augmenting path* is the minimum residual capacity of any arc in this path.

Obviously, whenever there is an augmenting path in the residual network $G(\mathbf{x})$ the flow $\mathbf{x}$ is not optimal. This motivates the following generic augmenting path algorithm:

algorithm Ford–Fulkerson
begin
Initially set $x_{ij} := 0,\ x_{ji} := 0$ for all $(i, j) \in A$;
do
construct residual network R with capacities r_{ij};
if there is an augmenting path from s to t in G' **then**
begin
Let $r_{\min}$ the minimum capacity of r along this path;
Increase the flow in N along the path by a value of $r_{\min}$;
end
until no such path from s to t in G' is found;

This algorithm is polynomial in the number of lattice sites if the distribution of capacities is discrete (binary for instance). In the general case it has to be improved, and there are indeed more efficient algorithms to solve this problem in polynomial time [1–3]. We stop the description of these algorithms and focus on the results we obtained by applying them to the particular elastic manifold model we are interested in here.

We performed the ground state calculation for the Hamiltonian (13) on $L^3 \times H$ hyper-cubic lattices for $L \leqslant 32$. H, the size in the extra direction, is taken to be larger than the interface width. We present the results for an exponential distribution for $J > 0$, $P(J) = \mathrm{e}^{-J/J_0}/J_0$ and uniform distribution for $0 \leqslant V_R \leqslant V_{\max}$. The disorder strength is controlled with the parameter $\Delta \equiv V_{\max}/J_0$. Other distributions studied include (bimodal, bimodal) and (uniform, uniform) distributions for (J, V_R), and gave identical estimates for the critical exponents.

The order parameter that provides the information about the suspected roughening transition is the magnetization-like quantity $m \equiv \langle|\langle \mathrm{e}^{\mathrm{i}\pi h_{\mathbf{x}}}\rangle_o|\rangle$, which is non-zero in the flat phase and vanishes in the rough phase. The critical point Δ_{c} can be determined from the finite-size-scaling property of the order parameter,

$$m(L, \varepsilon) = L^{-\beta/\nu}\mathcal{F}(\varepsilon L^{1/\nu}) \tag{16}$$

where $\varepsilon \equiv \Delta - \Delta_{\mathrm{c}}$, and β (ν) is the order parameter (correlation length) exponent. The scaling function $\mathcal{F}(x)$ has a limiting behaviour $\mathcal{F}(x \to 0) = \text{const}$ so that the order parameter decays algebraically with L as $m \sim L^{-\beta/\nu}$ at the critical point. It also behaves as $\mathcal{F}(x \to -\infty) \sim |x|^{\beta}$ so that $m \sim |\varepsilon|^{\beta}$ for $\Delta < \Delta_{\mathrm{c}}$ in the infinite system size limit.

Consider the effective exponent $[\beta/\nu](L) = -\log(m(2L)/m(L))/\log 2$. It converges to the value of β/ν at the critical point and deviates from it otherwise as L increases. We estimate the critical threshold as the optimal value of Δ at which the effective exponent approaches a non-trivial value. The plot for this effective exponent is shown in figure 8. One can see that there is a downward and upward curvature for $\Delta < 4.20$ and $\Delta > 4.30$, respectively. From this behaviour we estimate that $\Delta_{\mathrm{c}} = 4.25 \pm 0.05$ and $\beta/\nu = 0.07 \pm 0.03$.

Note that the effective exponent varies with L even at the estimated critical point, which implies that corrections to scaling are not negligible for system sizes up to $L = 32$. For that reason our numerical results for Δ_{c} and β/ν have rather large error bars, and one may need larger system sizes for better precision. The exponents β and ν could also be obtained from the scaling analysis using equation (16). We fix the values of Δ_{c} and β/ν to the values obtained before and vary ν to have an optimal data collapse. We obtain $\nu = 1.4 \pm 0.2$ and the corresponding scaling plot is shown in figure 8. The order parameter scaling property shows that the roughening phase transition is a *continuous* transition, though the exponent $\beta \simeq 0.1$ is very small, as opposed to the results of the Gaussian variational study [18] predicting a first-order transition.

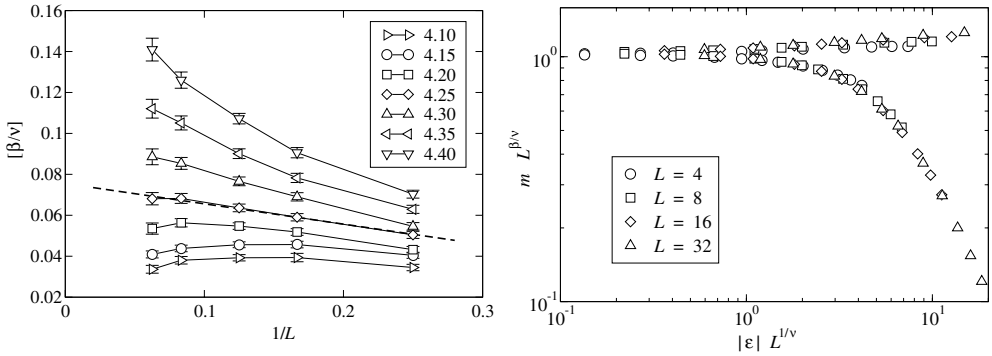

Figure 8. Left: the effective exponent $[\beta/\nu](L)$ for different values of Δ as a function of $1/L$. The broken line is a guide for the eyes that separates the curves with a downward bending ($\Delta < \Delta_c$) from those with an upward bending ($\Delta > \Delta_c$). Right: scaling plot of $mL^{\beta/\nu}$ versus $|\varepsilon|L^{1/\nu}$ with $\varepsilon = \Delta - 4.25$, $\beta/\nu = 0.07$ and $\nu = 1.4$.

6. Summary

To conclude we discussed several applications of polynomial combinatorial optimization algorithms to the numerical investigation of ground state properties of disordered systems. We did not touch the application of matching algorithms, with which one can compute the ground states of spin glass models on planar graphs (e.g. in 2D with free boundary conditions [23, 24] and to study 2D disordered elastic media [25]. We also did not discuss the optimization of sub-modular function, which is useful in the context of the $q \to \infty$ limit of the 2D random bond Potts model [26]. Together with the example we presented in this paper we learn that there are plenty of interesting problems in the realm of the theory of disordered systems that can be effectively studied with *polynomial* algorithms. There is another plentitude of problems that are currently investigated with *non-polynomial* combinatorial optimization algorithms (like the notorious 3D spin glass problem [3]), but this important topic is treated in another contribution to this special issue.

Acknowledgments

I thank M Alava, F O Pfeiffer, J D Noh, R Paul, V Petäjä and R Schorr for the fruitful collaborations on the issues discussed in this paper. This work was financially supported by the Deutsche Forschungsgemeinschaft (DFG), the European Science Foundation (ESF) within the SPHINX network and the European Union within the DYGLAGEMEM network.

References

[1] Rieger H 1998 *Lecture Notes in Physics* vol 501 ed J Kertesz and I Kondor (Berlin: Springer) pp 122–58
[2] Alava M, Duxbury P, Moukarzel C and Rieger H 2000 *Phase Transition and Critical Phenomena* vol 18 ed C Domb and J L Lebowitz (Cambridge: Academic) pp 141–317
[3] Hartmann A and Rieger H 2002 *Optimization in Physics* (Darmstadt: Wiley)
[4] Halpin-Healy T and Zhang Y-C 1995 *Phys. Rep.* **254** 215
[5] Peng C-K, Havlin S, Schwartz M and Stanley H E 1991 *Phys. Rev.* A **44** 2239
Pang N-N, Yu Y-K and Halpin-Healy T 1995 *Phys. Rev.* E **52** 3224
[6] Marsili M and Zhang Y-C 1998 *Phys. Rev.* E **57** 4814
Schwartz N, Nazaryev A L and Havlin S 1998 *Phys. Rev.* E **58** 7642

[7] Schorr R and Rieger H 2003 *Eur. Phys. J.* **33** 347
[8] For a review see Blatter G *et al* 1994 *Rev. Mod. Phys.* **66** 1125
[9] Doi M and Edwards S F 1986 *The Theory of Polymer Dynamics* (Oxford: Oxford University Press)
[10] Drossel B and Kardar M 1996 *Phys. Rev.* E **53** 5861
[11] Bikbov R and Nechaev S 2001 *Phys. Rev. Lett.* **87** 150602
[12] Petäjä V, Alava M and Rieger H 2003 *Preprint* cond-mat/0302509
[13] Rieger H and Blasum U 1997 *Phys. Rev.* B **55** 7394R
Pfeiffer F and Rieger H 2000 *J. Phys. A: Math. Gen.* **33** 2489
[14] Bokil H S and Young A P 1995 *Phys. Rev. Lett.* **74** 3021
[15] Kisker J and Rieger H 1998 *Phys. Rev.* B **58** R8873
Pfeiffer F and Rieger H 1999 *Phys. Rev.* B **60** 6304
[16] Pfeiffer F O and Rieger H 2002 *J. Phys.: Condens. Matter* **14** 2361
Pfeiffer F O and Rieger H 2003 *Phys. Rev.* E **67** 056113
[17] Nattermann T 1990 *Phys. Rev. Lett.* **64** 2454
Giarmachi T and Le Doussal P 1994 *Phys. Rev. Lett.* **72** 1530
Giarmachi T and Le Doussal P 1995 *Phys. Rev.* B **52** 1242
[18] Bouchaud J-P and Georges A 1992 *Phys. Rev. Lett.* **68** 3908
[19] Emig T and Nattermann T 1997 *Phys. Rev. Lett.* **79** 5090
Emig T and Nattermann T 1999 *Eur. J. Phys.* B **8** 525
[20] Seppälä E T, Alava M J and Duxbury P M 2001 *Phys. Rev.* E **63** 036126
[21] Noh J D and Rieger H 2001 *Phys. Rev. Lett.* **87** 176102
Noh J D and Rieger H 2002 *Phys. Rev.* E **66** 036117
[22] Middleton A A 1995 *Phys. Rev.* E **52** R3337
[23] Kawashima N and Rieger H 1997 *Europhys. Lett.* **39** 85
[24] Hartmann A K and Young A P 2002 *Phys. Rev.* B **66** 094419
Hartmann A K, Bray A J, Carter A C, Moore M A and Young A P 2002 *Phys. Rev.* B **66** 224401
[25] Middleton A A 2000 *Phys. Rev.* B **61** 14787
[26] Angles d'Auriac J-Ch, Igloi F, Preissmann M and Sebo A 2002 *Preprint* cond-mat/0204055
Angles d'Auriac J-Ch and Iglói F 2002 *Preprint* cond-mat/0211543

Endnotes

(1) Author: Please be aware that the colour figures in this article will only appear in colour in the Web version. If you require colour in the printed journal and have not previously arranged it, please contact the Production Editor now.